



Contents lists available at ScienceDirect

## Arabian Journal of Chemistry

journal homepage: [www.ksu.edu.sa](http://www.ksu.edu.sa)LED-driven photodeposition of Pt nanoparticles on TiO<sub>2</sub>: Combined effects of titania crystallinity and adopted wavelength on photoactivityAdam Kubiak<sup>a,\*</sup>, Maria Vittoria Dozzi<sup>b</sup>, Marco Montalbano<sup>b</sup>, Michał Cegłowski<sup>a</sup><sup>a</sup> Adam Mickiewicz University, Poznan, Faculty of Chemistry, Uniwersytetu Poznańskiego 8, PL-61614 Poznan, Poland<sup>b</sup> Dipartimento di Chimica, Università Degli Studi di Milano, Via C. Golgi 19, I-20133 Milano, Italy

## ARTICLE INFO

## Keywords:

Titanium dioxide  
Platinum  
Photodeposition  
LED  
Photooxidation

## ABSTRACT

Amidst the ongoing LED technology-driven energy revolution, it's crucial to re-examine how certain processes work. For this purpose, the present study dives into a new way of depositing platinum nanoparticles onto titania via photodeposition using LED light, carefully controlling the process by irradiating with different wavelengths. This novel approach has helped us to understand how the chosen wavelength may affect the properties of the synthesized materials, especially in relation to the shape of photodeposited nanoparticles. Moreover, the photodeposition method herein presented was proven to allow the nucleation and growth of Pt over amorphous titania, effectively expanding the application range of photodeposition. Importantly, the prepared samples were found to be highly effective at photocatalytically breaking down recalcitrant pharmaceutical drugs such as naproxen. This work significantly contributes to our understanding on how these materials can be used for technological applications such as photocatalysis, making it a noteworthy addition to the research field.

## 1. Introduction

The rapid growth of industrialization, as well as of global population, has led to an increase in the environmental pollution of water due to the discharge of noxious chemicals, often resulting as a consequence of both humane and industrial activities (Carpenter et al., 1998; Dudgeon et al., 2006; Järup, 2003). The serious threat to the development of a sustainable society posed by water pollution has driven researchers to seek for effective and green technologies aimed at remediating wastewaters (Fujishima et al., 2007; Hoffmann et al., 1995). Among those, heterogeneous photocatalysis has been proven to be a remediation process characterized by a number of advantages, such as i) the possibility to ensure a complete mineralization of the substrates without waste disposal issues; ii) the relatively low costs and iii) the opportunity to operate under mild conditions (Bhatkhande et al., 2002; Li et al., 2018). Nonetheless, photocatalysis is also particularly suited for the degradation of recalcitrant compounds such as pharmaceutical drugs (Mestre and Carvalho, 2019; Murgolo et al., 2021; Sharma et al., 2023; Velem-pini et al., 2021), for whose several conventional degradation methods (e.g., physical, chemical, and biological abatement technologies) are not efficient enough to be practically employed (Sharma et al., 2023).

The efficiency of photocatalytic remediation processes, however, are

directly tied to the efficiency of the employed photocatalyst material. For example, the performance of titanium dioxide, the most widely utilized semiconductor photocatalyst, is restrained by its two main drawbacks, represented by its wide band gap, requiring the use of highly energetic UV radiation to trigger the activation of the material, and by the high recombination rate of charge carriers photogenerated on it, causing the loss of energy provided by the absorbed photons in the form of heat (Guo et al., 2019; Nakata and Fujishima, 2012; Schneider et al., 2014). Over the course of the years, different strategies, such as TiO<sub>2</sub> morphology control (Dozzi et al., 2021; Dozzi and Selli, 2013a; Maisano et al., 2016) or doping with transition metals or *p*-block elements (Basavarajappa et al., 2020; Dozzi and Selli, 2013b; Kumaravel et al., 2019), have been explored to overcome such limitations. Among these, the deposition of noble metal (NM) nanoparticles (NPs) over the surface of titanium dioxide represents an attractive strategy which, by forming a Schottky barrier at the metal/semiconductor heterojunction, is capable of improving the performance of titanium dioxide in photocatalysis by dampening the recombination rate of photogenerated charge carriers (Bowker et al., 2022; Dozzi et al., 2017, 2009). In fact, by trapping electrons within noble metal nanoparticles, positively and negatively charged carriers result to be physically separated, thus limiting their recombination rate within the semiconductor.

\* Corresponding author.

E-mail address: [adam.kubiak@amu.edu.pl](mailto:adam.kubiak@amu.edu.pl) (A. Kubiak).<https://doi.org/10.1016/j.arabjc.2024.105846>

Received 21 March 2024; Accepted 26 May 2024

Available online 27 May 2024

1878-5352/© 2024 The Author(s). Published by Elsevier B.V. on behalf of King Saud University. This is an open access article under the CC BY license (<http://creativecommons.org/licenses/by/4.0/>).

Nonetheless, the efficiency of NM NPs deposition process has been reported to be heavily influenced by the adopted method (Dimitratos et al., 2016; Dozzi et al., 2009; Prati and Villa, 2011), with several different routes, e.g., deposition-precipitation (DP) (Dozzi et al., 2009; Tsubota et al., 1991; Zanella et al., 2002) and grafting (Dozzi et al., 2017; Liu et al., 2011), being proposed and investigated by researchers over the past years. Among them, the photodeposition method have attracted a lot of attention in photocatalysis. For example, uniquely from other techniques, photodeposition has been repeatedly reported to provoke a specific, preferential growth of Au nanoparticles over oxygen-defective TiO<sub>2</sub> surface sites, whereas in the case of Pt, NM NPs were evenly distributed on the surface of the metal oxide semiconductor, their growth being unaffected by the presence of specific surface defects (Gong et al., 2008; Kydd et al., 2007; Melvin et al., 2015). Moreover, it allows for the so-called “structure-directed photodeposition”, i.e., the deposition of NM NPs on specific crystal facets or peculiar branches on nanostructured materials (Wenderich and Mul, 2016).

Despite photodeposition has copiously proven to be capable of yielding enticing semiconductor photocatalyst materials, the fairly limited understanding of the physical-chemistry underneath an apparently simple photo-induced redox process makes the optimization of photodeposition in literature still largely empirical (Wenderich and Mul, 2016). In this juncture, studies investigating the effects of experimental parameters (e.g., solution pH, type of metallic precursor, temperature, and so on) are fundamental to fine-tune optimized experimental parameters aimed at obtaining the best cost-effective metal/semiconductor composites through photodeposition. Yet, the influence of the wavelength of the incident light employed during the photodeposition process has been rarely studied. Thus, we decided to investigate possible effects induced by the use of light with different wavelength ( $\lambda$ ) on the photodeposition of Pt over TiO<sub>2</sub>, changing the irradiation  $\lambda$  by employing LED lights with different maximum emission (280, 360, 450 and 550 nm). The following study aims at expanding the knowledge provided by our previously published research, which preliminarily explored photodeposition of Pt NPs on TiO<sub>2</sub> and graphite (Kubiak et al., 2023, 2022), by delving into the effects played by modifying either the LED-light employed during the photodeposition and the crystallinity of the TiO<sub>2</sub> support. In doing so, the photoactivity of the materials was tested in the photocatalytic degradation of naproxen, used as model molecule to evaluate the ability of the synthesized composite materials to photocatalytically degrade recalcitrant pharmaceutical drugs from contaminated waters.

## 2. Experimental part

### 2.1. Materials

Commercial anatase (nanopowder, <25 nm particle size; Sigma-Aldrich, 99,7%), titanium(IV) isopropoxide (Thermo Scientific, 97 %), chloroplatinic acid hexahydrate (Thermo Scientific, ACS reagent,  $\geq 37.50$  % Pt basis), methanol (Sigma-Aldrich, ACS reagent,  $\geq 99.8$  %), ammonia solution (Fisher Chemical, 25 %), isopropanol (Sigma-Aldrich, 99.5 %), naproxen sodium (Acros, >98 %). All reagents were of analytical grade and used without any further purification. The water used in all experiments was deionized.

### 2.2. Synthesis of TiO<sub>2</sub>-Pt materials

TiO<sub>2</sub>-Pt materials were synthesized using the photodeposition method with LED light. The procedure involved the dispersion of 1 g of anatase TiO<sub>2</sub> in 100 ml of 1:1 water/methanol solution. Subsequently, 300  $\mu$ l of chloroplatinic acid hydrate (0.1 wt% solution) were added to achieve a Pt/TiO<sub>2</sub> ratio of 1 wt%. The mixture was then sealed and purged with argon for 30 min. The suspension was irradiated for 1 h with monochromatic LED light with maximum emission at specific wavelengths, i.e. 280, 315, 365, 450, 550, and 650 nm or with

polychromatic high-pressure Hg lamp. During the process, a color change from orange (resulting from the presence of the platinum precursor) to gray was observed, indicating the successful Pt(IV) photoreduction to metallic platinum nanoparticles (NPs). The samples were thus labeled as TiO<sub>2</sub>-Pt\_Xnm with X referring to the maximum emission wavelength (in nm) of the LED adopted during the photodeposition procedure.

Selected samples were also prepared using amorphous TiO<sub>2</sub> synthesized using the method described elsewhere (Siwińska-Stefańska et al., 2018) and reported in the Supplementary Materials. The so-obtained samples were labeled as TiO<sub>2</sub>(Am)-Pt\_Xnm. Reference samples (TiO<sub>2</sub>Xnm) were synthesized following the same procedure except for the addition of the platinum precursor.

The light intensity of the Hg lamp on the reactor was measured to be approximately 20 mW/cm<sup>2</sup>. The adopted LEDs were thus calibrated to ensure comparable light intensity (ca. 20 mW/cm<sup>2</sup>).

### 2.3. Characterization of fabricated materials

Crystal structure analysis was performed using X-ray diffraction (XRD) with a Rigaku Miniflex 600 instrument (Rigaku, Japan). Cu K $\alpha$  radiation ( $\lambda = 1.5418$  Å) was used, collecting diffraction patterns in the 20-80° 2 $\theta$  range. The obtained patterns were analyzed using the Rietveld method implemented in the FullProf suite.

Diffuse reflectance spectroscopy (DRS) was employed to evaluate the light absorption properties of the oxide materials. The measurements were conducted using a Jasco V-670 spectrophotometer equipped with a PIN-757 integrating sphere, using barium sulfate as a reference standard. Reflectance (R) spectra in the 200–800 nm region, with a 1 nm spectral resolution, were converted into absorption (A) spectra using the relation  $A = 1-R$ .

The BET specific surface area (SSA), pore volume, and pore diameter of samples were determined by performing low-temperature nitrogen sorption measurements on a Quantachrome Autosorb iQ porosimeter from Quantachrome (USA). Prior to the measurements, the samples underwent degassing at 120 °C for 4 h. The surface area was determined using the multipoint BET method by analyzing the adsorption data in the relative pressure ( $p/p_0$ ) range of 0.05–0.30.

Transmission electron microscopy (TEM) analysis was carried out with FEI TECNAI G2 F20 electron microscope of the Unitech COSPECT at the University of Milan, operating at an accelerating voltage of 200 kV, with a Gatan CCD camera allowing high-resolution imaging. Few mg of the specimens were sonicated in 2-propanol and then transferred as a suspension on a copper grid covered with a holey carbon film. Micrographs were taken after solvent evaporation, spanning over the whole region of the sample, to achieve a truly representative statistical mapping of the investigated materials.

The actual photodeposited platinum content was determined by ICP-OES analysis, using a Varian 710-ES ICP optical emission spectrometer (Varian, USA) upon digestion in aqua regia (3:1 HCl:HNO<sub>3</sub>) of 15 mg of each sample.

X-ray Photoelectron Spectroscopy (XPS) experiments were carried out using a Specs UHV spectrometer (SPECS, Germany) equipped with a charge neutralizer. The binding energies were calibrated using the C 1s peak at 284.8 eV as a reference.

Photoluminescence (PL) analysis was performed using a spectrofluorometer (Fluorolog version-3, Horiba, Japan) equipped with a 450 W high-pressure xenon arc lamp as light source. The excitation spectra for the precursor were acquired by operating with emission wavelengths at 450 nm and 530 nm. For TiO<sub>2</sub>-Pt materials, emission spectra were acquired by operating with a 350 nm excitation wavelength. Spectral resolution and slit width were set to 2 nm and 2 mm, respectively.

## 2.4. Photocatalytic activity

### 2.4.1. Home-made LED-based light source

The LED light source employed during the photocatalytic tests was based on the combination of single-power LEDs emitting in the 365–370, 380–385, 395–400, and 420–430 nm wavelength ranges (BRIDGELUX, USA). The diodes were placed on an aluminum heat sink using thermally conductive glue (AG TermoGlue, Poland), and then connected in series. Finally, the LEDs were combined with an LED driver (MeanWell, Taiwan) to give a power of 10 W, which was confirmed using a GB202 wattmeter (GreenBule, China). The emission spectrum of the tailor-made LED light source is shown in Fig. S1.

### 2.4.2. Photocatalytic activity test

The photocatalytic activity of homemade samples was tested in aqueous suspensions, employing naproxen (NPX) as organic and model pharmaceutical degradation substrate.

The irradiated 0.1 L aqueous suspensions always contained 1 g/L of photocatalyst and an initial NPX concentration equal to 20 mg/L. The adsorption/desorption equilibrium of the substrate on the photocatalyst surface was attained within a black box under magnetic stirring (IKA Werke GmbH, Germany) for 30 min, before starting irradiation. Stirring was continued during the photocatalytic runs, irradiating the reaction mixture with the above-described custom-made LED setup. Portions (3 mL) of the suspension were thus withdrawn from the photoreactor at different time intervals during the runs and filtrated using a syringe filter (Macherey-Nagel, Germany). The supernatant was analyzed for residual NPX content by spectrophotometric analysis at 330 nm, the maximum absorption wavelength of NPX, employing a UV-2550 Shimadzu spectrophotometer instrument. To assess the photocatalytic efficiency of the investigated materials, the degradation yield ( $W$ ) was computed using the following formula:

$$W(\%) = \left(1 - \frac{C_t}{C_0}\right) \cdot 100\% \quad (1)$$

where  $C_0$  and  $C_t$  represent the initial NPX amount and the concentration of NPX determined upon a fixed irradiation time, respectively.

### 2.4.3. MS measurements

In order to better identify byproducts deriving from the NPX photocatalytic oxidation attained with the differently prepared TiO<sub>2</sub>-based samples, MS measurements were conducted on selected irradiated aqueous suspensions (upon proper filtration). The ESI-MS spectra were obtained using a Bruker amaZon SL (Germany) ion trap equipped with an electrospray ion source in infusion mode. The sample solution was introduced into the ionization source at a flow rate of 5  $\mu\text{L min}^{-1}$  through a syringe pump. The instrument was operated in the “enhanced resolution mode” with a mass range of 50–30000  $m/z$  and a scanning rate of 8100  $m/z$  per second. The capillary voltage was set to + 4.5 kV, and the endplate offset was –500 V. The temperature of the ion source was maintained at 80 °C, while the desolvation temperature was set to 250 °C. Nitrogen was used as the cone gas, while helium was used as desolvating gas with flow rates of 800 L·h<sup>-1</sup> and 50 L·h<sup>-1</sup>, respectively. The mass spectrometer was used in both positive and negative ionization modes.

## 3. Results and discussion

### 3.1. Characterization of Pt precursor solution

In order to get insights into the LED-induced photodeposition mechanism of platinum nanoparticles on TiO<sub>2</sub> surface, the light-induced excitation properties of the Pt precursor solution, adopted during photoreduction experiments, have been firstly studied. In particular, the excitation spectrum acquired by fixing the emission wavelength at 530

nm and reported in Fig. 1a clearly demonstrates that the chosen platinum precursor, H<sub>2</sub>PtCl<sub>6</sub>, can indeed be efficiently excited over a broad spectrum of wavelengths, ranging from UV-B to blue light, i.e. two distinct primary excitation peaks being clearly located at 365 nm and 450 nm. It's worth reminding that the H<sub>2</sub>PtCl<sub>6</sub> precursor solution may also exhibit light absorption at 262 nm, as evidenced by its absorption spectrum (Fig. S2). Moreover, based on the emission spectrum acquired at the fixed 450 nm excitation wavelength and reported in Fig. 1b, a single broad emission band spanning from 480 to 600 nm was observed.

### 3.2. Characterization of fabricated TiO<sub>2</sub>-Pt nanomaterials

#### 3.2.1. X-ray diffraction (XRD)

Fig. 2a shows the XRD patterns of bare anatase and TiO<sub>2</sub>-Pt nanomaterials. Clearly, the  $2\theta$  positions of the diffraction peaks within the recorded patterns of all synthesized samples perfectly match those of pure anatase (card no. 9009086) (Chung et al., 2020; Lin and Wang, 2019). Furthermore, diffraction peaks related to other TiO<sub>2</sub> crystal phases such as rutile or brookite were not observed, indicating that the synthesized materials were fully composed of anatase. Within the TiO<sub>2</sub>-Pt series, an additional peak was observed at  $2\theta = 39.8^\circ$  (see Fig. 2b), which could be attributed to the (1 1 1) planes of metallic platinum (card no. 1011107) (Lakshmanareddy et al., 2019; Ofiarska et al., 2016). The presence of this additional peak originating from Pt NPs was not observed in the case of TiO<sub>2</sub>-Pt<sub>650</sub> nm sample. The presence of Pt NPs diffraction peaks in the diffraction patterns suggests the effective deposition of nanocrystalline Pt particles on the materials surface, possibly organized in clusters large enough to give rise to characteristic diffraction signals of appreciable intensity. Importantly, no shifts in the TiO<sub>2</sub> pattern peaks were observed upon Pt loading, thus indicating that Pt is not incorporated into the lattice of TiO<sub>2</sub>, but rather deposited onto the oxide surface. Despite the relatively low noble metal content (1 wt%) in the materials under investigation, the presence of metallic Pt phases is clearly confirmed through XRD analysis. Typically, the absence of diffraction peaks related to noble metals in XRD patterns of metal-modified semiconductors indicates a high level of noble metal nanoparticle dispersion (Bielan et al., 2021; Zielińska-Jurek et al., 2015). This is significant because even highly crystalline noble metal nanoparticles in their fully reduced metallic states may not produce diffraction peaks if they are well-dispersed. This is because the coherent diffraction domain might be too small to generate a significant diffraction signal. Conversely, when noble metal nanoparticles are clustered together and not well-dispersed, the coherent diffraction domain can become the size of the clusters themselves, resulting in noticeable diffraction peaks in the patterns. However, XRD patterns of amorphous TiO<sub>2</sub>(Am)-Pt series samples did not exhibit any Pt diffraction peaks. Instead, the typical diffraction pattern of nanometer-sized x-ray amorphous TiO<sub>2</sub> is clearly observed (Fig. S3, see Supplementary Materials), fully in line with the data reported by Zhang et al. (Zhang et al., 2008).

Interestingly, the here adopted LED-induced Pt photodeposition process did not produce any variation, independently on the chosen LED wavelength, on both the fully anatase TiO<sub>2</sub> crystalline phase composition and the ca. 20 nm TiO<sub>2</sub> crystallites size of the starting TiO<sub>2</sub> sample. At the same time, no appreciable differences have been exhibited by the XRD patterns of the reference TiO<sub>2</sub>-Xnm samples (see Fig. S4 in the Supplementary Materials), thus excluding any potential influence solely exerted on the TiO<sub>2</sub> crystal structure by the employed photodeposition procedure upon irradiating with any of the chosen LED wavelengths (Grabowska et al., 2016).

#### 3.2.2. Diffuse reflection spectroscopy (DRS)

UV–vis absorption spectra of TiO<sub>2</sub>-Pt-Xnm and TiO<sub>2</sub>(Am)-Pt-Xnm series samples are collected in Fig. 3. Pt-modified powders show the typical broad, almost constant absorption extending over the entire visible region. The obtainment of pretty similar DRS spectra indirectly confirmed the deposition of similar Pt content among the investigated

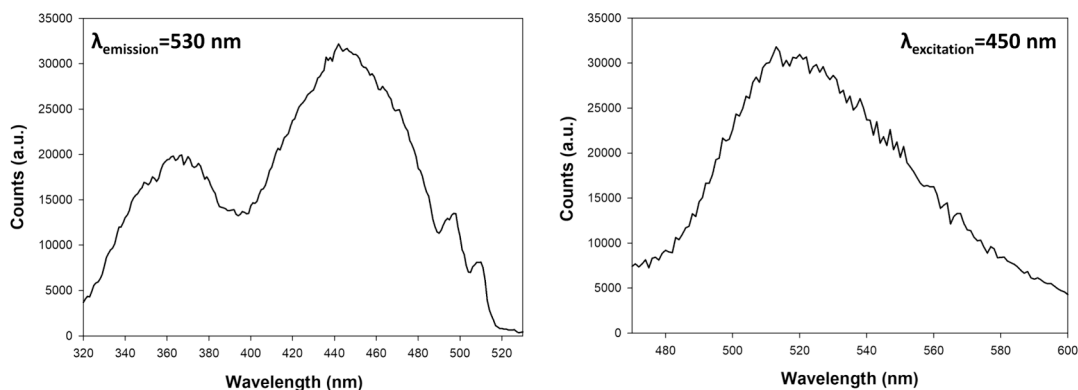


Fig. 1. Excitation and emission spectra of  $\text{H}_2\text{PtCl}_6$  solution, viewed from the right.

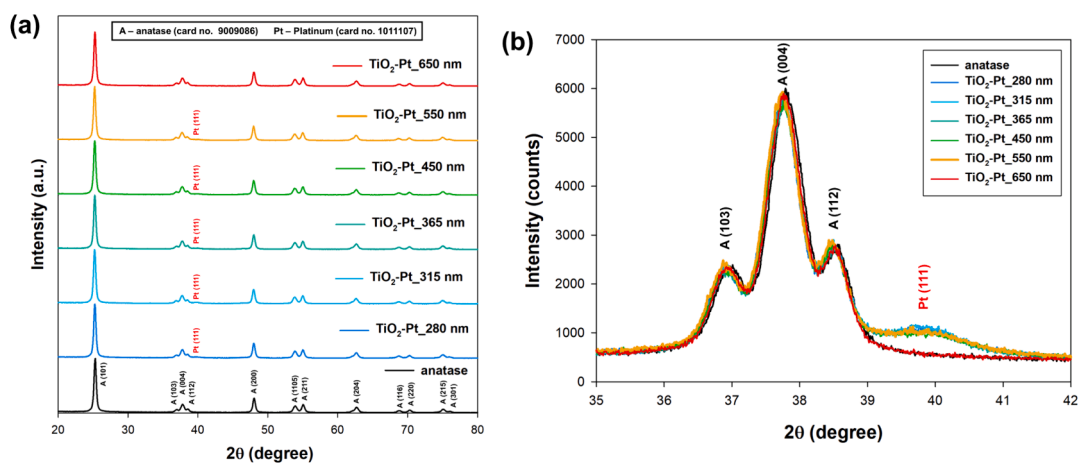


Fig. 2. (a) XRD patterns of  $\text{TiO}_2\text{-Pt-Xnm}$  series materials; (b) enlarged portion of the samples patterns, showing the peak associated to metallic platinum.

Pt-containing samples, except for the  $\text{TiO}_2\text{-Pt}_{650}$  nm material, whose spectrum only reveals the presence of an additional absorption band at approximately 400–450 nm, which can be attributed to the Pt precursor species adsorbed on the  $\text{TiO}_2$  surface (Guaraldo et al., 2015). It is important to note that this observation aligns with previous findings, indicating that the use of red light (650 nm wavelength) for the photodeposition process does not result in the reduction of Pt ions into fully metallic Pt NPs (Alamelu and Jaffar Ali, 2018). At the same time, as expected, the applied photodeposition process did not alter the band gap energy of the starting  $\text{TiO}_2$  material.

### 3.2.3. Specific surface area (SSA) determination

BET surface area values obtained for the  $\text{TiO}_2\text{-Pt}$  series samples are reported in Table S1 in Supplementary Materials, together with their calculated mean pore volume and size/diameter. Representative nitrogen adsorption-desorption isotherms acquired for home-made  $\text{TiO}_2\text{-Pt-Xnm}$  series materials can be found in Fig. S5 of the Supplementary Materials.

The nitrogen adsorption isotherms exhibited characteristic features of type IV, with a hysteresis loop observed at higher pressure values (Muttakin et al., 2018). Regardless of the analyzed nanomaterial, the hysteresis loop exhibited a type H3 behavior, typical of pores originating from the packing of spherically-shaped crystallites (Sing, 1982). Importantly, the process of platinum photodeposition on the anatase surface did not have any significant impact on the amount of adsorbed nitrogen, though a slight BET area increase (ca. 4–8 %) was observed for the  $\text{TiO}_2\text{-Pt-Xnm}$  materials compared to the bare anatase and the  $\text{TiO}_2\text{-Pt}_{650}$  nm samples. Regardless, all materials were characterized by a similar SSA, in the 73–82  $\text{m}^2 \text{g}^{-1}$  range, allowing to directly compare

their photocatalytic activities without differences in surface exposure affecting the relative performance of the photocatalysts.

### 3.2.4. HR-TEM analysis

To understand if the morphology of Pt nanoparticles photodeposited on  $\text{TiO}_2$  may be somehow influenced by the adopted LED wavelength, the noble metal particle size distribution (PSD) was thus determined acquiring high-resolution TEM images, collected in Fig. 4.

Interestingly, both shape and dispersion of Pt NPs anchored on anatase surface were found to be critically influenced by the LED wavelength. The irradiation of anatase  $\text{TiO}_2$  with high energy photons (e.g., 280 nm) allowed the deposition of almost spherically shaped Pt clusters, with variable sizes ranging from 20 to 60 nm, and composed of very small noble metal nanoparticles with average diameter of ca.  $3.2 \pm 0.7$  nm (Fig. 4a). The use of UV-A radiation (365 nm) guaranteed a more homogeneous dispersion on  $\text{TiO}_2$  surface of Pt NPs with mean size of ca.  $3.4 \text{ nm} \pm 0.8$  nm. Notably, no noble metal nanoparticle clusters were detected in the so-prepared sample, suggesting a different photodeposition mechanism (Fig. 4b). A quite similar degree of Pt NPs dispersion on  $\text{TiO}_2$  was also observed for the material obtained by irradiating with 450 nm LED light, i.e.  $\text{TiO}_2\text{-Pt}_{450}$  nm sample exhibiting a homogeneous distribution of Pt nanoparticles with mean diameter of  $4.0 \pm 1.0$  nm, although some irregularly (pear-like) shaped Pt NPs started to appear on the metal oxide semiconductor (Fig. 4c). However, the use of green light (550 nm) ensured the photodeposition of Pt NPs with mean diameter of ca.  $3.0 \pm 0.5$  nm, which clearly tend to aggregate forming Pt nanoclusters with quite homogenous/regular size (i.e. mean diameter of ca. 15–20 nm), apparently embedded between oxide particles (Fig. 4d).

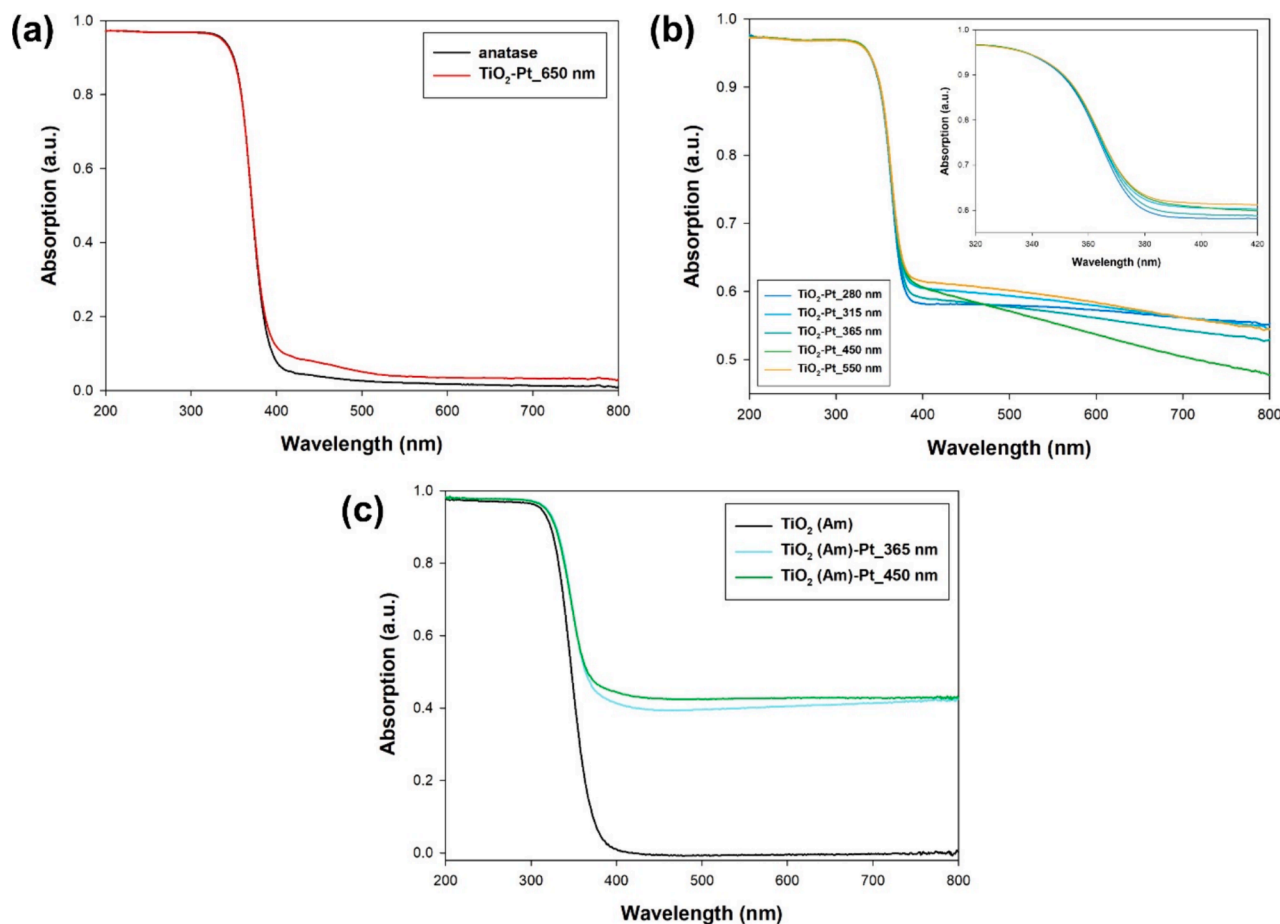


Fig. 3. DRS spectra of (a,b)  $\text{TiO}_2\text{-Pt}_X\text{nm}$ , and (c)  $\text{TiO}_2(\text{Am})\text{-Pt}_X\text{nm}$  series samples.

Furthermore, in order to investigate the role eventually played by the  $\text{TiO}_2$  crystallinity on Pt NPs photodeposition,  $\text{TiO}_2(\text{Am})\text{-Pt}_X\text{nm}$  series samples were also examined. The corresponding TEM images can be found in Fig. S6 of the Supplementary Materials. In particular, only  $\text{TiO}_2(\text{Am})\text{-Pt}$  samples prepared by using 365 and 450 nm LED wavelengths exhibited quite diluted Pt nanoclusters (mean diameter of 20 nm), composed of Pt nanoparticles units with ca.  $3.1 \pm 0.5$  nm size, i.e. no nanoparticles with Pt in metallic form being observed in the case of materials prepared by irradiating with other considered LED wavelengths (see 3.2.5. section). Moreover, it's important to underline a key point: as the  $\text{H}_2\text{PtCl}_6$  precursor is better excited within the blue light range, the 450 nm wavelength appears more suitable than 365 nm for photodepositing Pt on amorphous  $\text{TiO}_2$ . Thus, choosing blue-centered wavelength might be pivotal for achieving an optimized Pt nanocluster dispersion on x-ray amorphous  $\text{TiO}_2$ .

When comparing our findings with the existing scientific literature, it is crucial to highlight some significant differences. Firstly, previous studies have suggested that the photodeposition process generally enables a homogenous size distribution of noble metal NPs on the whole semiconductor surface. The dispersion of Pt NPs with homogeneous size distribution was particularly attained upon irradiation at specific LED wavelengths (365 nm and 450 nm). Interestingly, as shown in Fig. 4a, irradiation with high-energy photons at 280 nm can lead to irregular clustering of Pt nanoparticles. While this specific sample ( $\text{TiO}_2\text{-Pt}_{280}$  nm) was prepared using monochromatic LED light at 280 nm, similar effects might be also expected with polychromatic light sources including high-energy photons (UV-C).

Consequently, to address this important issue, we thus prepared an additional sample by following the same synthetic procedure, but in the presence of a polychromatic light source, i.e. a high-pressure Hg-lamp.

TEM images of the so obtained sample, named as  $\text{TiO}_2\text{-Pt}_{\text{poly}}$ , are provided in Fig. 5. Interestingly, the use of a conventional light source, specifically a high-pressure mercury lamp, led to a quite inhomogeneous Pt deposition throughout the entire synthesized sample. In particular, either Pt NPs (mean diameter of  $4.0 \text{ nm} \pm 0.5 \text{ nm}$ ) aggregated into nanoclusters (mean diameter of approximately 25 nm) or dispersed as single (and almost spherically shaped) units, with mean  $3.0 \pm 0.5$  nm diameter, were observed on the  $\text{TiO}_2\text{-Pt}_{\text{poly}}$  sample. So, by considering our previous observations along with this new finding, it becomes clear that the irradiation wavelength adopted during the photodeposition process may strongly affect the anchoring of Pt NPs on  $\text{TiO}_2$  surface in terms of both size and shape distribution.

### 3.2.5. Surface composition analysis

The actual amount of Pt co-catalyst deposited on the photocatalysts surface was quantitatively determined via ICP-OES analysis (Table 1). In particular, in the case of crystalline anatase, the here employed LED-driven photodeposition led to the fixation on the  $\text{TiO}_2$  surface of the nominal Pt loading only when irradiating with wavelengths in the 280–550 nm range. Differently, irradiation with 650 nm photons allowed to anchor only a small fraction of platinum, likely to be ascribed to residual amounts of adsorbed Pt precursor species rather than to Pt NPs produced via photoreduction. Interestingly, differently than crystalline anatase, a quantitative loading of reduced Pt NPs was never achieved on amorphous  $\text{TiO}_2$ . Therefore, the crystallinity of the titanium dioxide support seems to be required in order to gain the complete loading of Pt NPs by means of the here employed photodeposition with LEDs.

XPS analysis was used to determine the surface composition and oxidation state of elements in the  $\text{TiO}_2\text{-Pt}$  systems. High resolution XPS

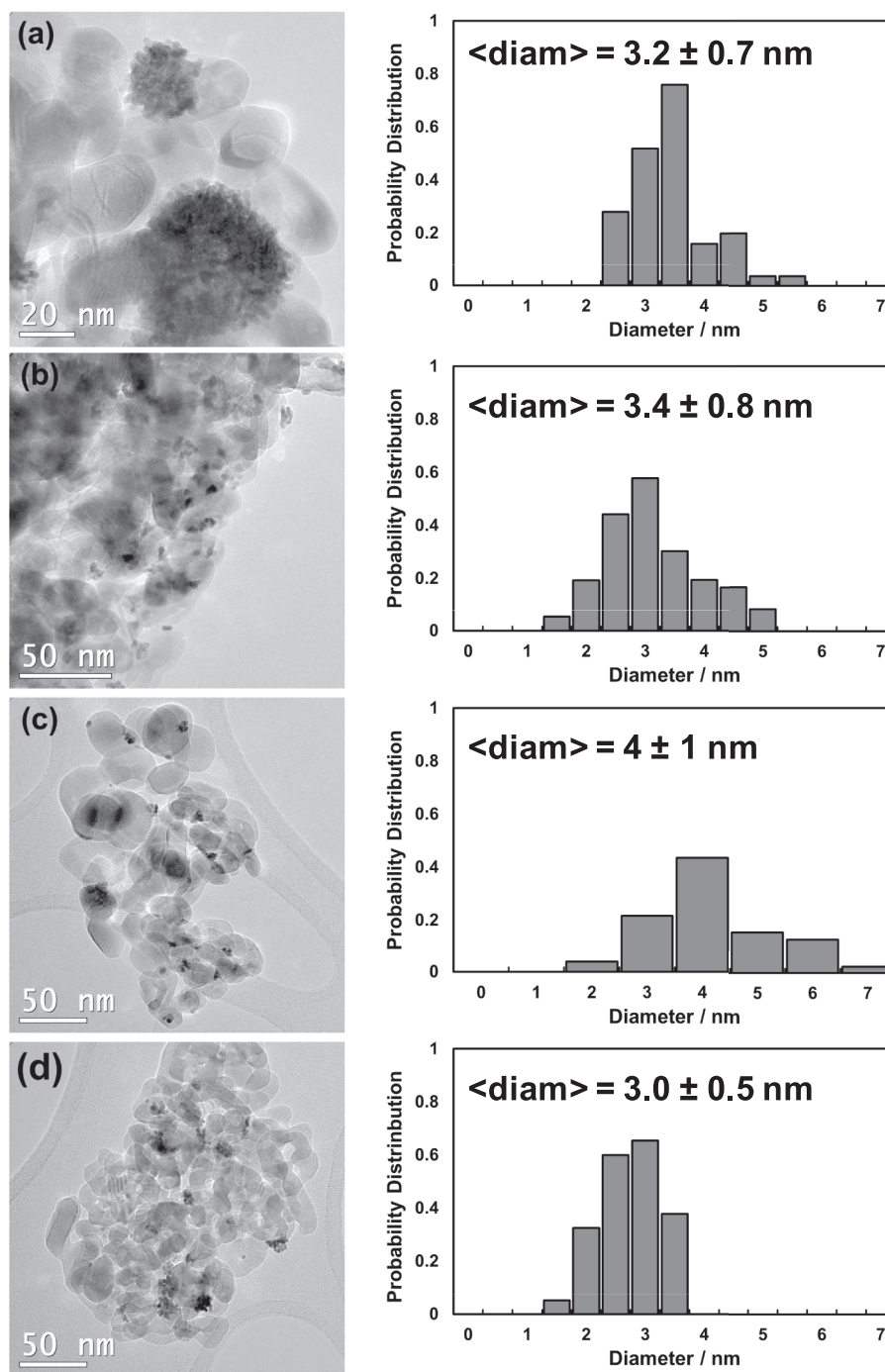


Fig. 4. TEM images and Pt NPs size distribution of  $\text{TiO}_2\text{-Pt}_X\text{nm}$  materials irradiated using (a) 280, (b) 365, (c) 450 and (d) 550 nm LED wavelength.

spectra in the Ti 2p and Pt 4f BE regions of the investigated  $\text{TiO}_2\text{-Pt}$  materials are reported in Fig. 6.

First of all, almost identical Ti 2p doublet signals, with two components at binding energy (BE) 458.5 and 464.2 eV, assigned to Ti 2p<sub>3/2</sub> and Ti 2p<sub>1/2</sub>, respectively, were recorded with both bare anatase and Pt-modified samples (Güzelçimen et al., 2020; Jensen et al., 2005). The absence of any modifications of Ti 2p peaks in terms of both shape and energy position with respect to the standard ones indirectly exclude any possible incorporation of Pt into the  $\text{TiO}_2$  lattice structure.

The Pt 4f region spectrum was analyzed and fitted with a doublet, with a separation of 3.33 eV between the Pt 4f<sub>7/2</sub> and Pt 4f<sub>5/2</sub> peaks. The mainline Pt 4f<sub>7/2</sub> peak was observed at a binding energy of 71.1 eV, indicating the presence of metallic platinum on the surface (Haselmann

et al., 2020; Zhang et al., 2020). Differently, it is crucial to emphasize that the obtention of such XPS Pt peak signal at relatively higher BE (ca. 73 eV) for the  $\text{TiO}_2\text{-Pt}_{650 \text{ nm}}$  sample demonstrated the presence of oxidized platinum in the form of adsorbed precursor on the surface of such photocatalyst. This finding supports previous research showing that 650 nm LED light does not reduce the platinum precursor to its metallic phase.

Interestingly, all the here adopted physico-chemical characterization techniques (XRD, DRS, TEM and XPS) clearly confirmed the impossibility to deposit Pt NPs on crystalline  $\text{TiO}_2$  by applying the photo-deposition technique with low energy photons (650 nm). For this reason, the photoactivity of the  $\text{TiO}_2\text{-Pt}_{650 \text{ nm}}$  sample will not be evaluated in any photocatalytic activity test (Section 3.4).

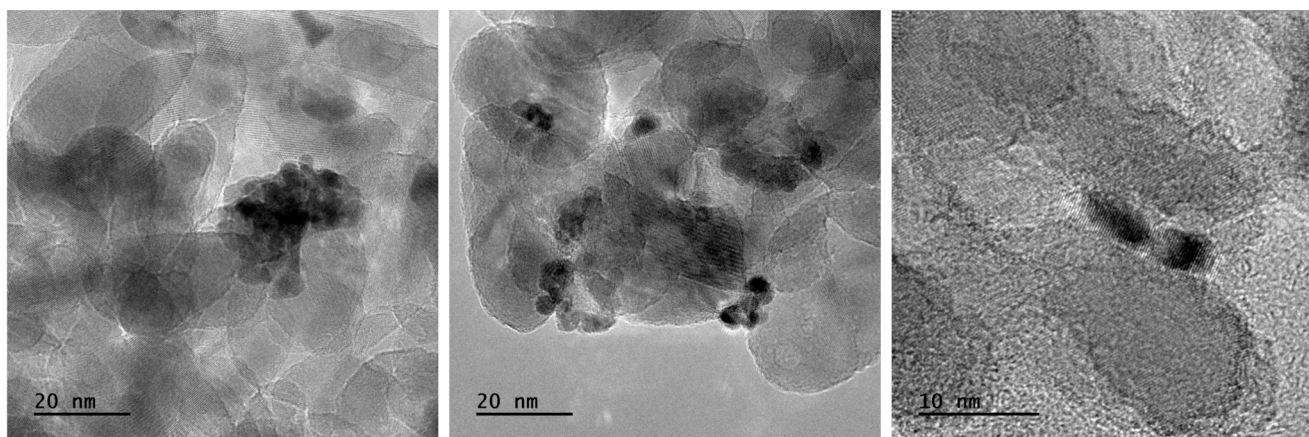


Fig. 5. TEM images of TiO<sub>2</sub>-Pt<sub>poly</sub> sample, i.e. prepared by using polychromatic high-pressure Hg-lamp.

Table 1

Pt amount (wt.%) deposited on the surface of the investigated photocatalysts, determined by ICP-OES analysis.

Sample	ICP-OES Pt (%)
TiO <sub>2</sub> -Pt_280 nm	0.9 (±0.1)
TiO <sub>2</sub> -Pt_315 nm	0.9 (±0.1)
TiO <sub>2</sub> -Pt_365 nm	1.1 (±0.1)
TiO <sub>2</sub> -Pt_450 nm	1.0 (±0.1)
TiO <sub>2</sub> -Pt_550 nm	1.0 (±0.1)
TiO <sub>2</sub> -Pt_650 nm	0.3 (±0.1)
TiO <sub>2</sub> (Am)-Pt_365 nm	0.6 (±0.1)
TiO <sub>2</sub> (Am)-Pt_450 nm	0.5 (±0.1)

Fig. 7 shows XPS spectra obtained for TiO<sub>2</sub>-Pt materials synthesized with the use of amorphous TiO<sub>2</sub>. Interestingly, the XPS spectra obtained in the Pt 4f region for the TiO<sub>2</sub>(Am)-Pt\_365nm and TiO<sub>2</sub>(Am)-Pt\_450nm samples, following deconvolution, mainly reveal the presence of species attributable to adsorbed noble metal precursor, although low intense XPS signals associated to Pt(0) species (ca. 71.1 eV) also confirmed the presence of small amount of metallic Pt NPs on amorphous TiO<sub>2</sub>, in line with HR-TEM analysis.

This finding strongly suggests that the platinum precursor and/or the semiconductor oxide can be somehow excited, thus ensuring the partial fixation of Pt NPs even on the surface of amorphous TiO<sub>2</sub> materials. However, it is important to note that the efficiency of this process on an amorphous semiconductor is significantly lower compared to that occurring on crystalline materials. This is likely attributed to the fact that amorphous TiO<sub>2</sub> may be strongly affected by undesired photo-generated charge carriers recombination, thereby lowering the efficiency of the Pt precursor species photoreduction.

### 3.2.6. Photoluminescence (PL) spectroscopy

Steady-state PL spectroscopy was preliminary performed to understand if and how the electron transfer paths from the excited semiconductor to the Pt NPs may be somehow influenced by the LED wavelength adopted during the photodeposition process and/or the crystalline nature of the starting TiO<sub>2</sub> photocatalyst. Fig. 8 reports the PL signals of Pt-modified TiO<sub>2</sub> samples compared to that of the corresponding bare material in terms of intensity and shape profile upon excitation at 350 nm.

It is necessary to remind that TiO<sub>2</sub> is an indirect semiconductor, so its emission signal resulting from the recombination of conduction band (CB) electrons with valence band (VB) holes is expected to be very weak at room temperature (Wu et al., 2019). So, fast electron – hole recombination process, being detrimental for the overall photocatalytic efficiency of TiO<sub>2</sub>-based materials, largely occurs producing heat instead of

radiative emission. Previous works have clearly evidenced that shape, intensity and dynamic PL profile of TiO<sub>2</sub> materials may be somehow affected by the introduction of localized defect states in the TiO<sub>2</sub> structure, e.g. by doping or by applying specific surface treatments under aerobic or anaerobic conditions (Esrafilii et al., 2022). New range of intra band gap states may behave as trapping sites of photoproduced charge carriers, thus significantly affecting the overall electron – hole recombination dynamics and originating more intense and longer-living PL component (Giannakas et al., 2017). The here investigated TiO<sub>2</sub> material exhibited PL signal in the 400 – 450 nm range, which may be assigned to the radiative recombination of bulk self-trapped excitons at intrinsic TiO<sub>6</sub> octahedra of anatase crystal structure (Dudziak et al., 2021) (Fig. 8a).

All the Pt-containing materials systematically exhibited quite similar in shape, but less intense PL spectra compared to bare TiO<sub>2</sub>, as a consequence of the effective migration of electrons photopromoted in the TiO<sub>2</sub> CB (or at defective sites) towards the noble metal NPs (Xie et al., 2014). More interestingly, the largest PL decrease has been attained by the TiO<sub>2</sub>-Pt\_450 nm sample which, being characterized by homogeneously and well-dispersed Pt nanoparticles, may exhibit superior ability in capturing photoexcited electrons from TiO<sub>2</sub> compared to the TiO<sub>2</sub>-Pt\_280 nm sample, where Pt clusters were instead observed.

Similar observations were made for the TiO<sub>2</sub>(Am)-Pt series (Fig. 8b). Indeed, the photoluminescent emission of x-ray amorphous TiO<sub>2</sub>, also in this case originating from e-h pairs radiative annihilation, clearly proves that electron-hole pairs are indeed generated to a certain extent upon irradiation with light of suitable wavelength also in amorphous TiO<sub>2</sub>. This result, along with XRD patterns (Fig. S3), suggests that the here synthesized amorphous TiO<sub>2</sub> may be predominantly composed by very small (~2 nm size) nanoparticles with a highly distorted shell and a strained anatase-like core (Zhang et al., 2008). Nonetheless, the PL emission associated with charge carrier recombination was quenched upon Pt NPs photodeposition. In this case as well, the TiO<sub>2</sub>(Am)-Pt\_450 nm sample exhibited a relatively more marked PL suppression compared to the TiO<sub>2</sub>(Am)-Pt\_365 nm material, possibly as a consequence of the more efficient fixation of metallic Pt on amorphous TiO<sub>2</sub> surface attained by using blue light during the photodeposition process (as demonstrated by the previously reported XPS analyses).

Interestingly, these preliminary results demonstrate that the LED wavelength adopted during the photodeposition process may also specifically affect the relative degree of PL suppression, generally attained with noble metal-containing TiO<sub>2</sub>-based photocatalysts, thus determining a peculiar effect on the overall electron-hole recombination process.

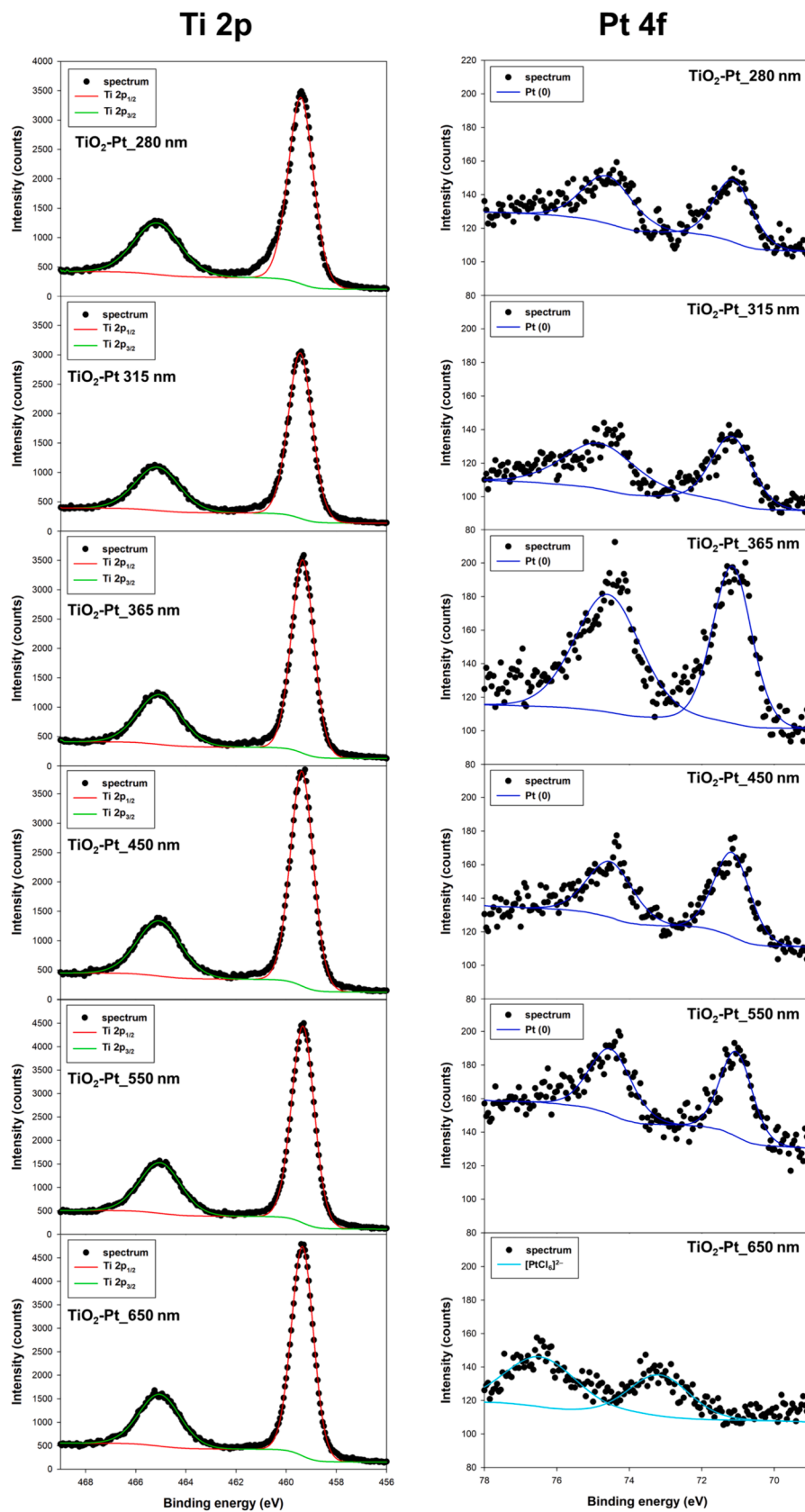


Fig. 6. High resolution XPS spectra of TiO<sub>2</sub>-Pt materials prepared using different LED wavelengths.

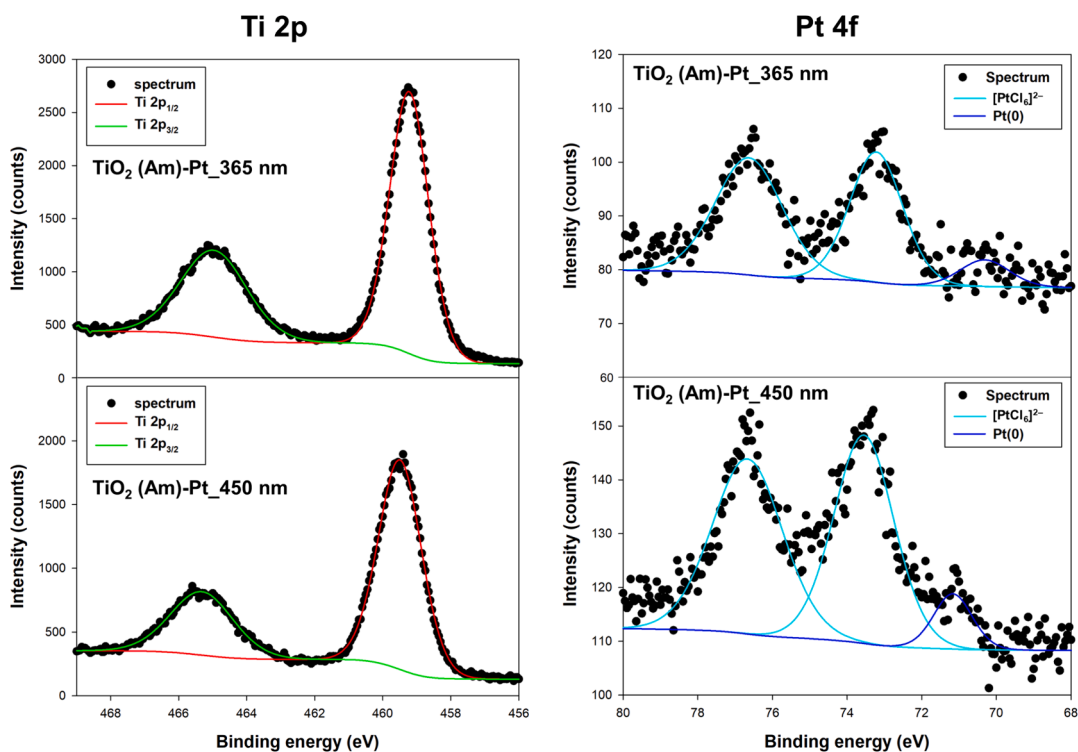


Fig. 7. XPS spectra of  $\text{TiO}_2(\text{Am})\text{-Pt}$  materials obtained using 365 or 450 nm LED wavelengths.

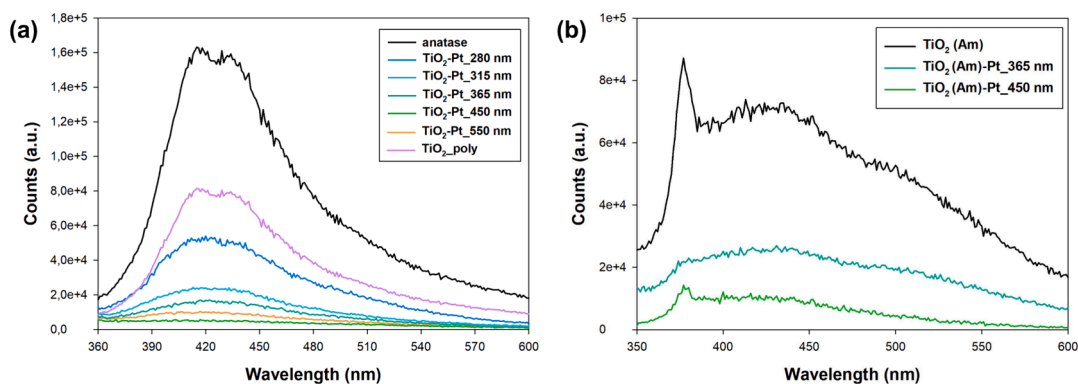


Fig. 8. Emission spectra of (a) crystalline and (b) amorphous  $\text{TiO}_2\text{-Pt}$  series samples, prepared using different LED wavelengths.

### 3.3. Proposed mechanism for LED-induced deposition of Pt nanoparticles

Based on the collected data, possible mechanisms of platinum photodeposition as a function of the adopted LED wavelength may be outlined. Specifically, UV-C light exposure results in the formation of differently sized platinum nanoclusters on the anatase surface (Alamelu and Jaffar Ali, 2018). In particular, the photodeposition method, initiated by high energy photons, corresponds to the already well-established working mechanism mainly based on the direct photoexcitation of the  $\text{TiO}_2$  photocatalyst (Ratliff et al., 2009). This is clearly demonstrated by the fact that 280 nm-mediated Pt NPs deposition did not occur on amorphous  $\text{TiO}_2$  materials, i.e. the excitation of noble metal precursor species contained in the starting aqueous suspension not being sufficient to ensure the Pt deposition. Nonetheless, the potential effects directly played by the UV-C light on the anatase surface shouldn't be overlooked. In fact, continuous UV light irradiation may directly alter the surface of titania by introducing new surface defects. Previous work by Stevanovic et al. (Stevanovic et al., 2012) noted that a photoluminescence band near 500 nm can act as a reliable indicator of UV-

triggered shifts in the band structure. Therefore, we also acquired the photoluminescence spectra of reference  $\text{TiO}_2$  Xnm samples, i.e. anatase samples exposed to the considered LED wavelengths in the absence of Pt precursor species (see Fig. S7 in the Supplementary Materials). Interestingly, the data clearly evidenced that only  $\text{TiO}_2$  materials irradiated with UV and especially UV-C radiation exhibited slightly more intense PL signals, possibly due to the light-induced introduction of surface defects, as further confirmed by the partial color change showed by such materials, turning from white into slightly gray. So, the surface defects directly introduced by UV exposure can serve as further electron-rich reactive sites promoting platinum precursors reduction, mirroring the "key and lock" analogy, which boosts the distribution of platinum nanoparticles on the  $\text{TiO}_2$  surface (Dessal et al., 2019; Sakthivel et al., 2004).

Differently, it is important to consider that 315 and 365 nm photons may promote the simultaneous photoactivation of anatase  $\text{TiO}_2$  and platinum precursor species ( $\text{H}_2\text{PtCl}_6$ ), possibly adsorbed on titania surface (Watanabe, 2017; Yan et al., 2016). Therefore, under such conditions, the deposition of Pt NPs may result from combined mechanisms

still mainly involving the transfer of photopromoted electrons (upon direct TiO<sub>2</sub> band-gap excitation) from the TiO<sub>2</sub> CB to the adsorbed Pt(IV) species, but also encountering the direct photoreduction of [PtCl<sub>6</sub>]<sup>2-</sup> complexes upon their photoactivation (Haidry et al., 2023; Sharma et al., 2016).

Furthermore, effects produced on the photodeposition process by TiO<sub>2</sub> irradiation with 450 nm and 550 nm LED wavelengths should be taken into account. In fact, these wavelengths aren't within anatase's absorption range (Fig. 3), indicating that photons with such energy impinging on the reaction slurry may directly photoexcite H<sub>2</sub>PtCl<sub>6</sub> precursor species, as demonstrated by its excitation spectrum clearly peaking at 450 nm (Fig. 1). Simultaneously, in line with previous report (Burgeth and Kisch, 2002) adsorption of H<sub>2</sub>PtCl<sub>6</sub> species on anatase TiO<sub>2</sub> may extend the light absorption properties of the resultant photocatalyst up to ca. 600 nm, as further supported by the UV-vis absorption spectrum of the TiO<sub>2</sub>-Pt\_650 nm reported in Fig. 3a. Interestingly, while the nominal Pt content was photodeposited on crystalline TiO<sub>2</sub> upon irradiation at 450 nm, the anchoring of Pt NPs only partially occurred on amorphous TiO<sub>2</sub> under the same experimental conditions.

In this scenario, the photoexcitation of Pt precursor species adsorbed especially on anatase TiO<sub>2</sub> may induce the transfer of electrons towards TiO<sub>2</sub> CB, while resultant oxidized Pt-precursor species may accept electrons from hole scavenger molecules, in this case methanol, added in the irradiated aqueous suspensions (Burgeth and Kisch, 2002.; Macyk et al., 2003). At the same time, the so-produced oxidized hole scavenger molecules, generally behaving as strongly reductant radical species, may also contribute to the noble metal precursor reduction into metallic Pt NPs. In fact, according to literature reports (Bernardini et al., 2010; Dozzi et al., 2009; Tantis et al., 2016), such photogenerated species, thanks to their highly negative redox potential, could either originate the so-called current doubling effect by injecting electrons into the semiconductor conduction band, or mediate the reduction of a wide variety of species adsorbed on the photocatalyst (in this case, adsorbed Pt precursor species, since the highly reducible O<sub>2</sub> has been removed from the reaction environment). Therefore, during the photodeposition process carried out by irradiation at 450 nm (and probably also at 550 nm for the crystalline TiO<sub>2</sub> material), Pt precursor reduction may proceed on the photocatalyst surface through the action of conduction band electrons, directly injected by the photoexcited Pt precursor species or by the photogenerated (and highly reductant) oxidized molecules derived by the added hole scavenger species (i.e. methanol).

Moreover, it results clear that the efficiency of the here proposed mechanism may be strongly affected by the TiO<sub>2</sub> crystallinity. In fact, amorphous TiO<sub>2</sub>, possibly dominated by detrimental charge carrier recombination, may not be sufficiently efficient in capturing and trapping electrons, provided by the reductant species described above,

which are essential to allow the stabilization of metallic Pt NPs on the semiconductor surface upon irradiation at 450 nm.

### 3.4. Photocatalytic activity

The photocatalytic degradation of naproxen, irradiating the photocatalysts using the tailor-made LED light source (Fig. S1), was chosen as test reaction to evaluate the photocatalytic performance of the synthesized TiO<sub>2</sub>-Pt materials. The obtained data in terms of naproxen degradation efficiency are reported in Fig. 9.

Firstly, among investigated samples, bare, metal-free anatase exhibited a relatively modest photoactivity compared to Pt-modified specimens, irrespective of the LED wavelength employed during the photodeposition synthesis.

However, notable differences were observed among the synthesized Pt-containing materials. In particular, the presence of Pt clusters on TiO<sub>2</sub>-Pt\_280 nm led to a less marked photoactivity increase in the photo-oxidation efficiency of naproxen compared to other LED-light synthesized materials. In particular, TiO<sub>2</sub>-Pt\_315 nm and TiO<sub>2</sub>-Pt\_365 nm samples exhibited a slightly enhanced photoactivity, possibly attributed to a better dispersion of Pt NPs on the surface of anatase. Achieving good interparticle contact is crucial for Pt to serve as active centers for capturing photogenerated electrons. Interestingly, TiO<sub>2</sub>-Pt\_450 nm and TiO<sub>2</sub>-Pt\_550 nm samples exhibited the highest photooxidative activity for naproxen removal among all the tested materials. These materials showed satisfactory dispersion of platinum on anatase surface, and the photodeposition process under visible light (TiO<sub>2</sub>-Pt\_450 nm and TiO<sub>2</sub>-Pt\_550 nm) did not induce any modification to the anatase structure (on the basis of PL analyses reported above). To provide a comparison, further naproxen photo-oxidation experiments in the presence of TiO<sub>2</sub>-Pt\_poly (i.e. the TiO<sub>2</sub>-Pt material prepared with a high-pressure mercury lamp) were performed. This particular material exhibited the lowest efficiency in removing the tested pharmaceutical. The reduced efficiency could be possibly attributed to the not optimized morphology and/or distribution of platinum NPs, hindering an efficient electron transfer from TiO<sub>2</sub> to Pt NPs (as supported by PL analysis – 3.2.6. Section).

Amorphous TiO<sub>2</sub> exhibited negligible photoactivity due to its inherent structural disorder, which fosters the recombination of charge carriers (Fig. 9b). Nonetheless, research by Chung et al. (Chung et al., 2021) has demonstrated that nitrogen modification can activate amorphous TiO<sub>2</sub> within the visible light spectrum. Similarly, Buddee et al. (Buddee et al., 2011) devised a method involving impregnation with chromium and iron, resulting in enhanced photocatalytic performance of amorphous TiO<sub>2</sub> for methyl blue degradation under both UV and visible light, outperforming commercial TiO<sub>2</sub>. Consequently, the

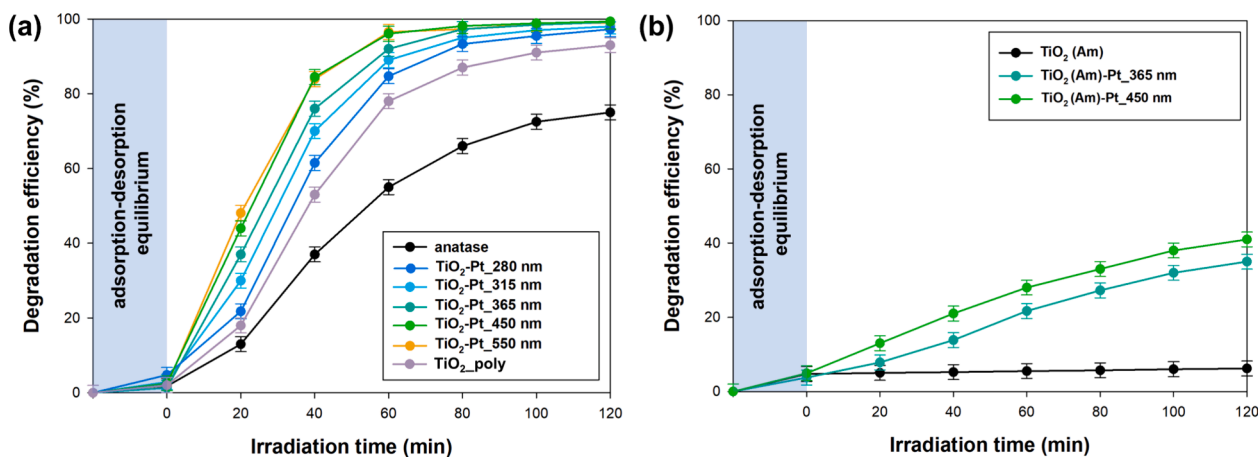


Fig. 9. Efficiency of naproxen photocatalytic degradation attained with (a) crystalline and (b) amorphous TiO<sub>2</sub>(Am)-Pt materials, using an innovative tailor-made LED photoreactor.

observed photocatalytic activity in the oxidation of naproxen employing amorphous TiO<sub>2</sub>-Pt composites should not be unexpected (Kattel et al., 2016). By these means, the presence of Pt nanoparticles facilitates excitation within the visible light range, prompting the generation of reactive oxygen species and curtailing recombination rates. The synergy of these phenomena contributes to the achieved efficiency of approximately 35–40 % in naproxen degradation after 2 h irradiation.

NPX, a stable organic compound composed of two aromatic rings, can be degraded by oxidizing species such as  $\cdot\text{O}_2^-$ ,  $\cdot\text{OH}$ , and  $\text{h}^+$  generated during the photocatalytic degradation process using either crystalline or amorphous TiO<sub>2</sub>-Pt systems (Ohtani et al., 1997). Aiming at better investigating the NPX degradation mechanism, the intermediate products formed during the photocatalytic reaction were analyzed using ESI mass spectrometry (MS).

In the TiO<sub>2</sub>-Pt photocatalytic system employed in this study, the degradation of NPX can be proposed as a decarboxylation reaction. Initially, the attack of  $\cdot\text{OH}$  radicals occurs at the methyl position of the naphthalene ring, leading to decarboxylation and the formation of TP1 ( $m/z$  185) and TP2 ( $m/z$  201) intermediates (Eslami et al., 2020). In another pathway, the oxidation of NPX is initiated by  $\text{h}^+$  and  $\cdot\text{O}_2^-$  attacking the carbon atoms with the most positive charge, resulting in the formation of carbon-centered radical species. These radicals further undergo decarboxylation and are transformed by  $\cdot\text{O}_2^-$  into TP1 ( $m/z$  185) and TP3 ( $m/z$  223) intermediates (Cheng et al., 2012). Additionally, decarboxylation can occur through valence band holes  $\text{h}^+$  attack at the C (1) position, leading to the formation of the TP4 ( $m/z$  158) intermediate (Muktaridha et al., 2021). Eventually, ring-opening reactions take place, resulting in the formation of products with  $m/z$  values of 134, 148, and 178 (Jiménez-Salcedo et al., 2022). These products further undergo oxidation and eventually transform into CO<sub>2</sub> and H<sub>2</sub>O. Furthermore, it is important to note that the degradation pathways of naproxen were found to be consistent across all the tested materials. Thus, it can be concluded that the LED wavelength used during the photodeposition process of platinum solely affects the efficiency of naproxen removal, without altering the actual degradation pathways. The proposed pathway for naproxen removal using TiO<sub>2</sub>-Pt photocatalysts is depicted in Fig. 10. The obtained ESI-MS spectra are presented in Table S2 in the Supplementary Materials.

#### 4. Conclusions

In the midst of the LED technology-driven energy revolution, a novel perspective emerges regarding the deposition of platinum nanoparticles onto titania using LED light. What sets this research apart is the exploration of the profound impact that different LED wavelengths can exert on the characteristics of photodeposited Pt NPs on the surface of anatase TiO<sub>2</sub>, especially in terms of shape and distribution. Furthermore, the research applied to amorphous TiO<sub>2</sub> has revealed that specific LED wavelengths lead to a diluted dispersion of Pt nanoclusters also on such TiO<sub>2</sub> material. In particular, the optimal Pt NPs distribution on full anatase TiO<sub>2</sub> has been attained upon irradiation with 365 or 450 nm monochromatic LED light, while the use of 280 or 550 nm provided the anchoring of clustered Pt NPs. Differently, in relation to amorphous TiO<sub>2</sub> samples, the partial deposition of Pt NPs, only in clustered form, exclusively occurred upon irradiation with 365 or 450 nm photons. Interestingly, possible mechanisms for platinum NPs photodeposition on either anatase or amorphous TiO<sub>2</sub> materials, involving different photo-activation paths in relation to the employed LED wavelength, have been reported.

Moreover, comprehensive testing has confirmed the remarkable efficacy of these TiO<sub>2</sub>-Pt materials in the photocatalytic degradation of substances like naproxen. In essence, this study not only offers valuable insights into the deposition of Pt nanoparticles on titania using LED light but also elucidates the intricate ways in which various wavelengths affect the process. This represents a significant contribution to the field, particularly in the domain of photocatalysis.

#### CRediT authorship contribution statement

**Adam Kubiak:** Writing – review & editing, Writing – original draft, Visualization, Validation, Supervision, Resources, Project administration, Methodology, Investigation, Funding acquisition, Formal analysis, Data curation, Conceptualization. **Maria Vittoria Dozzi:** Writing – review & editing, Writing – original draft, Formal analysis, Data curation, Conceptualization. **Marco Montalbano:** Writing – review & editing, Writing – original draft, Formal analysis, Data curation. **Michał Ceglowski:** Writing – review & editing, Supervision, Project administration.

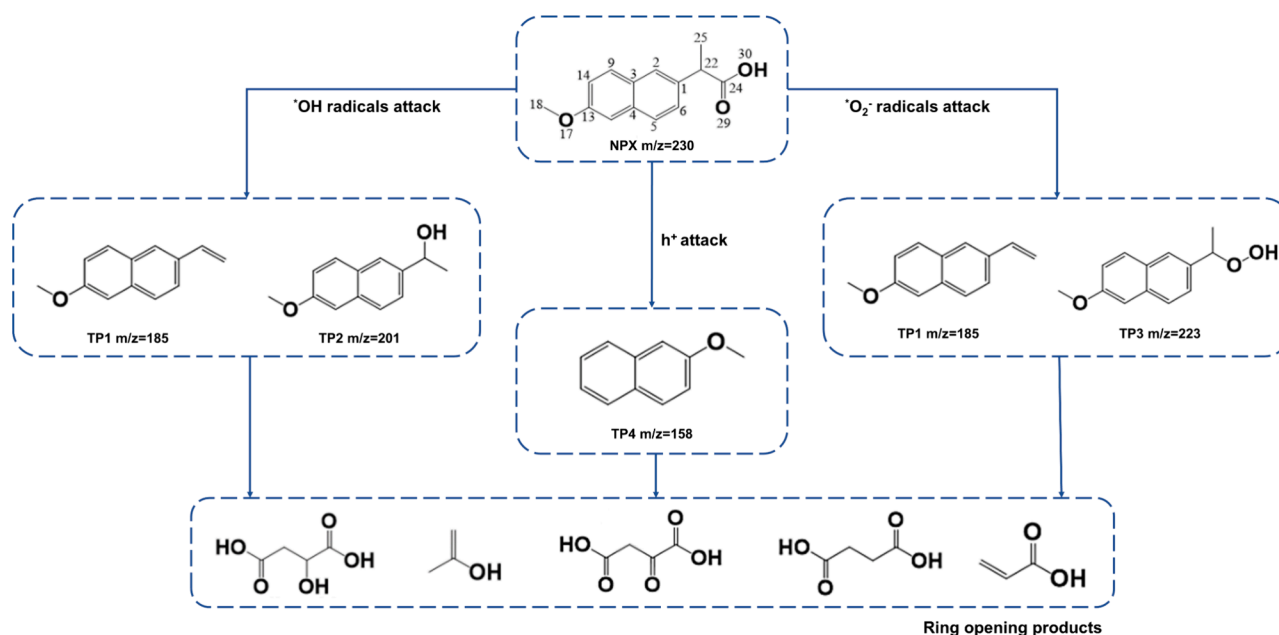


Fig. 10. Proposed degradation pathway of NPX in the presence of TiO<sub>2</sub>-Pt photocatalysts.

## Declaration of Competing Interest

The authors declare that they have no known competing financial interests or personal relationships that could have appeared to influence the work reported in this paper.

## Acknowledgments

This work was supported by the National Science Centre, Poland, under grant number 2023/07/X/ST5/00022. Unitech COSPECT Transmission Electron Microscope facility at Università degli Studi di Milano is gratefully acknowledged.

## Appendix A. Supplementary data

Supplementary data to this article can be found online at <https://doi.org/10.1016/j.arabjc.2024.105846>.

## References

- Alamelu, K., Jaffar Ali, B.M., 2018. TiO<sub>2</sub>-Pt composite photocatalyst for photodegradation and chemical reduction of recalcitrant organic pollutants. *J. Environ. Chem. Eng.* 6, 5720–5731. <https://doi.org/10.1016/j.jece.2018.08.042>.
- Basavarajappa, P.S., Patil, S.B., Ganganagappa, N., Reddy, K.R., Raghu, A.V., Reddy, C. V., 2020. Recent progress in metal-doped TiO<sub>2</sub>, non-metal doped/codoped TiO<sub>2</sub> and TiO<sub>2</sub> nanostructured hybrids for enhanced photocatalysis. *Int. J. Hydrogen Energy.* 45, 7764–7778. <https://doi.org/10.1016/j.ijhydene.2019.07.241>.
- Bernardini, C., Cappelletti, G., Dozzi, M.V., Selli, E., 2010. Photocatalytic degradation of organic molecules in water: Photoactivity and reaction paths in relation to TiO<sub>2</sub> particles features. *J. Photochem. Photobiol. A Chem.* 211, 185–192. <https://doi.org/10.1016/j.jphotochem.2010.03.006>.
- Bhatkhande, D.S., Pangarkar, V.G., Beenackers, A.A.C.M., 2002. Photocatalytic degradation for environmental applications - A review. *J. Chem. Technol. Biotechnol.* 77, 102–116. <https://doi.org/10.1002/jctb.532>.
- Bielan, Z., Kowalska, E., Dudziak, S., Wang, K., Ohtani, B., Zielińska-Jurek, A., 2021. Mono- and bimetallic (Pt/Cu) titanium(IV) oxide core-shell photocatalysts with UV/Vis light activity and magnetic separability. *Catal. Today* 361, 198–209. <https://doi.org/10.1016/j.cattod.2020.05.034>.
- Bowker, M., O'Rourke, C., Mills, A., 2022. The role of metal nanoparticles in promoting photocatalysis by TiO<sub>2</sub>. *Top. Curr. Chem.* 380, 17. <https://doi.org/10.1007/s41061-022-00373-x>.
- Buddee, S., Wongnawa, S., Sirimahachai, U., Puetpaibool, W., 2011. Recyclable UV and visible light photocatalytically active amorphous TiO<sub>2</sub> doped with M (III) ions (M = Cr and Fe). *Mater. Chem. Phys.* 126, 167–177. <https://doi.org/10.1016/j.matchemphys.2010.11.044>.
- Burgeth, G., Kisch, H., 2002. Photocatalytic and photoelectrochemical properties of titanium(IV) chloroplatinate(IV). *Coord. Chem. Rev.* 230, 41–47. [https://doi.org/10.1016/S0010-8545\(02\)00095-4](https://doi.org/10.1016/S0010-8545(02)00095-4).
- Carpenter, S.R., Caraco, N.F., Correll, D.L., Howarth, R.W., Sharpley, A.N., Smith, V.H., 1998. Nonpoint Pollution of Surface Waters with Phosphorus and Nitrogen. *Eco. Appl.* 8, 559–568. [https://doi.org/10.1890/1051-0761\(1998\)008\[0559:NPOSWW\]2.0.CO;2](https://doi.org/10.1890/1051-0761(1998)008[0559:NPOSWW]2.0.CO;2).
- Cheng, X., Yu, X., Xing, Z., Wan, J., 2012. Enhanced Photocatalytic Activity of Nitrogen Doped TiO<sub>2</sub> Anatase Nano-Particle under Simulated Sunlight Irradiation. *Energy Procedia* 16, 598–605. <https://doi.org/10.1016/j.egypro.2012.01.096>.
- Chung, Y.H., Han, K., Lin, C.Y., O'Neill, D., Mul, G., Mei, B., Yang, C.M., 2020. Photocatalytic hydrogen production by photo-reforming of methanol with one-pot synthesized Pt-containing TiO<sub>2</sub> photocatalysts. *Catal. Today.* 356, 95–100. <https://doi.org/10.1016/j.cattod.2019.07.042>.
- Chung, K.H., Kim, B.J., Park, Y.K., Kim, S.C., Jung, S.C., 2021. Photocatalytic properties of amorphous n-doped TiO<sub>2</sub> photocatalyst under visible light irradiation. *Catalysts.* 11, 1010. <https://doi.org/10.3390/catal11081010>.
- Dessal, C., Martínez, L., Maheu, C., Len, T., Morfin, F., Rousset, J.L., Puzenat, E., Afanasiev, P., Aouine, M., Soler, L., Llorca, J., Piccolo, L., 2019. Influence of Pt particle size and reaction phase on the photocatalytic performances of ultradispersed Pt/TiO<sub>2</sub> catalysts for hydrogen evolution. *J. Catal.* 375, 155–163. <https://doi.org/10.1016/j.jcat.2019.05.033>.
- Dimitratos, N., Villa, A., Prati, L., Hammond, C., Chan-Thaw, C.E., Cookson, J., Bishop, P. T., 2016. Effect of the preparation method of supported Au nanoparticles in the liquid phase oxidation of glycerol. *Appl. Catal. A Gen.* 514, 267–275. <https://doi.org/10.1016/j.apcata.2015.12.031>.
- Dozzi, M.V., Prati, L., Canton, P., Selli, E., 2009. Effects of gold nanoparticles deposition on the photocatalytic activity of titanium dioxide under visible light. *Phys. Chem. Chem. Phys.* 11, 7171–7180. <https://doi.org/10.1039/b907317e>.
- Dozzi, M.V., Selli, E., 2013b. Doping TiO<sub>2</sub> with p-block elements: Effects on photocatalytic activity. *J. Photochem. Photobiol. C* 14, 13–28. <https://doi.org/10.1016/j.jphotochemrev.2012.09.002>.
- Dozzi, M.V., Chiarello, G.L., Pedroni, M., Livraghi, S., Giamello, E., Selli, E., 2017. High photocatalytic hydrogen production on Cu(II) pre-grafted Pt/TiO<sub>2</sub>. *Appl. Catal. B.* 209, 417–428. <https://doi.org/10.1016/j.apcatb.2017.03.007>.
- Dozzi, M.V., Montalbano, M., Marra, G., Mino, L., Selli, E., 2021. Effects of anatase TiO<sub>2</sub> morphology and surface fluorination on environmentally relevant photocatalytic reduction and oxidation reactions. *Mater. Today Chem.* 22, 100624. <https://doi.org/10.1016/j.mtchem.2021.100624>.
- Dozzi, M.V., Selli, E., 2013a. Specific Facets-Dominated Anatase TiO<sub>2</sub>: Fluorine-Mediated Synthesis and Photoactivity. *Catalysts.* 3, 455–485. <https://doi.org/10.3390/catal3020455>.
- Dudgeon, D., Arthington, A.H., Gessner, M.O., Kawabata, Z.I., Knowler, D.J., Lévêque, C., Naiman, R.J., Prieur-Richard, A.H., Soto, D., Stiassny, M.L.J., Sullivan, C.A., 2006. Freshwater biodiversity: Importance, threats, status and conservation challenges. *Biol. Rev. Camb. Philos. Soc.* 81, 163–182. <https://doi.org/10.1017/S1464793105006950>.
- Dudziak, S., Kowalkińska, M., Karczewski, J., Pisarek, M., Siuzdak, K., Kubiak, A., Siwińska-Ciesielczyk, K., Zielińska-Jurek, A., 2021. Solvothermal growth of {001} exposed anatase nanosheets and their ability to mineralize organic pollutants: The effect of alcohol type and content on the nucleation and growth of TiO<sub>2</sub> nanostructures. *Appl. Surf. Sci.* 563, 150360. <https://doi.org/10.1016/j.apsusc.2021.150360>.
- Eslami, A., Amini, M.M., Asadi, A., Safari, A.A., Daglioglu, N., 2020. Photocatalytic degradation of ibuprofen and naproxen in water over NS-TiO<sub>2</sub> coating on polycarbonate: Process modeling and intermediates identification. *Inorg. Chem. Commun.* 115, 107888. <https://doi.org/10.1016/j.inoche.2020.107888>.
- Esrabili, A., Salimi, M., Jonidi Jafari, A., Reza Sobhi, H., Gholami, M., Rezaei Kalantary, R., 2022. Pt-based TiO<sub>2</sub> photocatalytic systems: A systematic review. *J. Mol. Liq.* 352, 118685. <https://doi.org/10.1016/j.molliq.2022.118685>.
- Fujishima, A., Zhang, X., Tryk, D.A., 2007. Heterogeneous photocatalysis: From water photolysis to applications in environmental cleanup. *Int. J. Hydrog. Energy.* 32, 2664–2672. <https://doi.org/10.1016/j.ijhydene.2006.09.009>.
- Giannakas, A.E., Antonopoulou, M., Papavasiliou, J., Deligiannakis, Y., Konstantinou, I., 2017. Photocatalytic performance of Pt-TiO<sub>2</sub>, Pt-N-TiO<sub>2</sub> and Pt-N/F-TiO<sub>2</sub> towards simultaneous Cr(VI) reduction/benzoic acid oxidation: Insights into photogenerated charge carrier dynamics and catalyst properties. *J. Photochem. Photobiol. A* 349, 25–35. <https://doi.org/10.1016/j.jphotochem.2017.08.066>.
- Gong, X.Q., Selloni, A., Dulub, O., Jacobson, P., Diebold, U., 2008. Small Au and Pt clusters at the anatase TiO<sub>2</sub> (101) surface: Behavior at terraces, steps, and surface oxygen vacancies. *J. Am. Chem. Soc.* 130, 370–381. <https://doi.org/10.1021/ja0773148>.
- Grabowska, E., Marchelek, M., Klimczuk, T., Trykowski, G., Zaleska-Medynska, A., 2016. Noble metal modified TiO<sub>2</sub> microspheres: Surface properties and photocatalytic activity under UV-vis and visible light. *J. Mol. Catal. A Chem.* 423, 191–206. <https://doi.org/10.1016/j.molcata.2016.06.021>.
- Guaraldo, T.T., De Brito, J.F., Wood, D., Zanon, M.V.B., 2015. A New Si/TiO<sub>2</sub>/Pt p-n Junction Semiconductor to Demonstrate Photoelectrochemical CO<sub>2</sub> Conversion. *Electrochim. Acta.* 185, 117–124. <https://doi.org/10.1016/j.electacta.2015.10.077>.
- Guo, Q., Zhou, C., Ma, Z., Yang, X., 2019. Fundamentals of TiO<sub>2</sub> Photocatalysis: Concepts, Mechanisms, and Challenges. *Advanced Materials* 31, 1901997. <https://doi.org/10.1002/adma.201901997>.
- Güzëlçimen, F., Tanören, B., Çetinkaya, Ç., Kaya, M.D., Efkere, H.İ., Özen, Y., Bingöl, D., Sirkeci, M., Kinaci, B., Ünlü, M.B., Özçelik, S., 2020. The effect of thickness on surface structure of rf sputtered TiO<sub>2</sub> thin films by XPS, SEM/EDS, AFM and SAM. *Vacuum.* 182, 109766. <https://doi.org/10.1016/j.vacuum.2020.109766>.
- Haidry, A.A., Ji, Y., Raza, A., Zhu, H., Zavabeti, A., Saruhan, B., 2023. Elucidating the hydrogen adsorption kinetics on Pt/TiO<sub>2</sub>/Pt based highly efficient sensors. *Mater. Res. Bull.* 167, 112415. <https://doi.org/10.1016/j.materresbull.2023.112415>.
- Haselmann, G.M., Baumgartner, B., Wang, J., Wieland, K., Gupta, T., Herzig, C., Limbeck, A., Lendl, B., Eder, D., 2020. In Situ Pt Photodeposition and Methanol Photooxidation on Pt/TiO<sub>2</sub>: Pt-Loading-Dependent Photocatalytic Reaction Pathways Studied by Liquid-Phase Infrared Spectroscopy. *ACS Catal.* 10, 2964–2977. <https://doi.org/10.1021/acscatal.9b05588>.
- Hoffmann, M.R., Martin, S.T., Choi, W., Bahnemann, D.W., 1995. Environmental Applications of Semiconductor Photocatalysis. *Chem. Rev.* 95, 69–96. <https://doi.org/10.1021/cr00033a004>.
- Järup, L., 2003. Hazards of heavy metal contamination. *Br. Med. Bull.* 68, 167–182. <https://doi.org/10.1093/bmb/ldg032>.
- Jensen, H., Soloviev, A., Li, Z., Søgaard, E.G., 2005. XPS and FTIR investigation of the surface properties of different prepared titania nano-powders. *Appl. Surf. Sci.* 246, 239–249. <https://doi.org/10.1016/j.apsusc.2004.11.015>.
- Jiménez-Salcedo, M., Monge, M., Tena, M.T., 2022. The photocatalytic degradation of naproxen with g-C<sub>3</sub>N<sub>4</sub> and visible light: Identification of primary by-products and mechanism in tap water and ultrapure water. *J. Environ. Chem. Eng.* 10, 106964. <https://doi.org/10.1016/j.jece.2021.106964>.
- Kattel, S., Yan, B., Chen, J.G., Liu, P., 2016. CO<sub>2</sub> hydrogenation on Pt, Pt/SiO<sub>2</sub> and Pt/TiO<sub>2</sub>: Importance of synergy between Pt and oxide support. *J. Catal.* 343, 115–126. <https://doi.org/10.1016/j.jcat.2015.12.019>.
- Kubiak, A., Varma, N., Sikorski, M., 2022. Insight into the LED-assisted deposition of platinum nanoparticles on the titania surface: understanding the effect of LEDs. *Sci. Rep.* 12, 22572. <https://doi.org/10.1038/s41598-022-27232-5>.
- Kubiak, A., Rozmanowski, T., Gabała, E., Krawczyk, P., 2023. Insight into the LED-induced deposition of Pt nanoparticles on a graphite matrix: Unravelling the photodeposition processes on materials different than semiconductors. *J. Photochem. Photobiol. A Chem.* 441, 114744. <https://doi.org/10.1016/j.jphotochem.2023.114744>.

- Kumaravel, V., Mathew, S., Bartlett, J., Pillai, S.C., 2019. Photocatalytic hydrogen production using metal doped TiO<sub>2</sub>: A review of recent advances. *Appl. Catal. B* 244, 1021–1064. <https://doi.org/10.1016/j.apcatb.2018.11.080>.
- Kydd, R., Chiang, K., Scott, J., Amal, R., 2007. Low energy photosynthesis of gold-titania catalysts. *Photochem. Photobiol. Sci.* 6, 829–832. <https://doi.org/10.1039/b703528d>.
- Lakshmanareddy, N., Navakoteswara Rao, V., Cheralathan, K.K., Subramaniam, E.P., Shankar, M.V., 2019. Pt/TiO<sub>2</sub> nanotube photocatalyst – Effect of synthesis methods on valance state of Pt and its influence on hydrogen production and dye degradation. *J. Colloid. Interface. Sci.* 538, 83–98. <https://doi.org/10.1016/j.jcis.2018.11.077>.
- Li, X., Xie, J., Jiang, C., Yu, J., Zhang, P., 2018. Review on design and evaluation of environmental photocatalysts. *Front Environ Sci Eng* 12, 14. <https://doi.org/10.1007/s11783-018-1076-1>.
- Lin, X., Wang, J., 2019. Green synthesis of well dispersed TiO<sub>2</sub>/Pt nanoparticles photocatalysts and enhanced photocatalytic activity towards hydrogen production. *Int. J. Hydrog. Energy*, 44, 31853–31859. <https://doi.org/10.1016/j.ijhydene.2019.10.062>.
- Liu, M., Qiu, X., Miyauchi, M., Hashimoto, K., 2011. Cu(II) oxide amorphous nanoclusters grafted Ti<sup>3+</sup> self-doped TiO<sub>2</sub>: An efficient visible light photocatalyst. *Chem. Mater.* 23, 5282–5286. <https://doi.org/10.1021/cm203025b>.
- Macyk, W., Burgeth, G., Kisch, H., 2003. Photoelectrochemical properties of platinum (IV) chloride surface modified TiO<sub>2</sub>. *Photochem. Photobiol. Sci.* 2, 322–328. <https://doi.org/10.1039/b211583b>.
- Maisano, M., Dozzi, M.V., Coduri, M., Artiglia, L., Granozzi, G., Selli, E., 2016. Unraveling the Multiple Effects Originating the Increased Oxidative Photoactivity of {001}-Facet Enriched Anatase TiO<sub>2</sub>. *ACS Appl. Mater. Interfaces*, 8, 9745–9754. <https://doi.org/10.1021/acsmi.6b01808>.
- Melvin, A.A., Illath, K., Das, T., Raja, T., Bhattacharyya, S., Gopinath, C.S., 2015. M-Au/TiO<sub>2</sub> (M = Ag, Pd, and Pt) nanophotocatalyst for overall solar water splitting: role of interfaces. *Nanoscale*, 7, 13477–13488. <https://doi.org/10.1039/c5nr03735b>.
- Mestre, A.S., Carvalho, A.P., 2019. Photocatalytic degradation of pharmaceuticals carbamazepine, diclofenac, and sulfamethoxazole by semiconductor and carbon materials: A review. *Molecules*, 24, 3702. <https://doi.org/10.3390/molecules24203702>.
- Muktaridha, O., Adlim, M., Suhendrayatna, S., Ismail, I., 2021. Progress of 3d metal-doped zinc oxide nanoparticles and the photocatalytic properties. *Arab. J. Chem.* 14, 103175 <https://doi.org/10.1016/j.arabj.2021.103175>.
- Murgolo, S., De Ceglie, C., Di Iaconi, C., Mascolo, G., 2021. Novel TiO<sub>2</sub>-based catalysts employed in photocatalysis and photoelectrocatalysis for effective degradation of pharmaceuticals (PhACs) in water: A short review. *Curr. Opin. Green Sustain. Chem.* 30, 100473 <https://doi.org/10.1016/j.cogsc.2021.100473>.
- Muttakin, M., Mitra, S., Thu, K., Ito, K., Saha, B.B., 2018. Theoretical framework to evaluate minimum desorption temperature for IUPAC classified adsorption isotherms. *Int. J. Heat. Mass. Transf.* 122, 795–805. <https://doi.org/10.1016/j.ijheatmasstransfer.2018.01.107>.
- Nakata, K., Fujishima, A., 2012. TiO<sub>2</sub> photocatalysis: Design and applications. *J. Photochem. Photobiol. C* 13, 169–189. <https://doi.org/10.1016/j.jpchemrev.2012.06.001>.
- Ofiarska, A., Pieczyńska, A., Fiszka Borzyszkowska, A., Stepnowski, P., Siedlecka, E.M., 2016. Pt-TiO<sub>2</sub>-assisted photocatalytic degradation of the cytostatic drugs ifosfamide and cyclophosphamide under artificial sunlight. *Chem. Eng. J.* 285, 417–427. <https://doi.org/10.1016/j.cej.2015.09.109>.
- Ohtani, B., Iwai, K., Nishimoto, S.-I., Sato, S., 1997. Role of Platinum Deposits on Titanium(IV) Oxide Particles: Structural and Kinetic Analyses of Photocatalytic Reaction in Aqueous Alcohol and Amino Acid Solutions. *J. Phys. Chem. B* 101, 3349–3359. <https://doi.org/10.1021/jp962060q>.
- Prati, L., Villa, A., 2011. The art of manufacturing gold catalysts. *Catalysts*, 2, 24–37. <https://doi.org/10.3390/catal2010024>.
- Ratliff, J.S., Tenney, S.A., Hu, X., Conner, S.F., Ma, S., Chen, D.A., 2009. Decomposition of dimethyl methylphosphonate on Pt, Au, and Au-Pt clusters supported on TiO<sub>2</sub> (110). *Langmuir*, 25, 216–225. <https://doi.org/10.1021/la802361q>.
- Sakthivel, S., Shankar, M.V., Palanichamy, M., Arabindoo, B., Bahnemann, D.W., Murugesan, V., 2004. Enhancement of photocatalytic activity by metal deposition: Characterisation and photonic efficiency of Pt, Au and Pd deposited on TiO<sub>2</sub> catalyst. *Water. Res.* 38, 3001–3008. <https://doi.org/10.1016/j.watres.2004.04.046>.
- Schneider, J., Matsuoka, M., Takeuchi, M., Zhang, J., Horiuchi, Y., Anpo, M., Bahnemann, D.W., 2014. Understanding TiO<sub>2</sub> Photocatalysis: Mechanisms and Materials. *Chem. Rev.* 114, 9919–9986. <https://doi.org/10.1021/cr5001892>.
- Sharma, A., Mehta, S.K., Singh, S., Gupta, S., 2016. Synthesized colloidal-supported Pt and bimetallic Pt–Mo nanoparticles as electrocatalyst in oxidation of methanol in alkaline solution. *J. Appl. Electrochem.* 46, 27–38. <https://doi.org/10.1007/s10800-015-0900-6>.
- Sharma, M., Yadav, A., Mandal, M.K., Dubey, K.K., 2023. TiO<sub>2</sub> based photocatalysis: a valuable approach for the removal of pharmaceuticals from aquatic environment. *Int. J. Environ. Sci. Technol.* 20, 4569–4584. <https://doi.org/10.1007/s13762-021-03894-y>.
- Sing, K.S.W., 1982. Reporting Physisorption Data for Gas/Solid Systems with Special Reference to the Determination of Surface Area and Porosity. *Pure Appl. Chem.* 57 (1982), 603–619. <https://doi.org/10.1351/pac198557040603>.
- Siwińska-Stefańska, K., Kubiak, A., Piasecki, A., Goscińska, J., Nowaczyk, G., Jurga, S., Jesionowski, T., 2018. TiO<sub>2</sub>/ZnO binary oxide systems: Comprehensive characterization and tests of photocatalytic activity. *Materials*, 11, 841. <https://doi.org/10.3390/ma11050841>.
- Stevanovic, A., Büttner, M., Zhang, Z., Yates, J.T., 2012. Photoluminescence of TiO<sub>2</sub>: Effect of UV light and adsorbed molecules on surface band structure. *J. Am. Chem. Soc.* 134, 324–332. <https://doi.org/10.1021/ja2072737>.
- Tantis, I., Dozzi, M.V., Bettini, L.G., Chiarello, G.L., Dracopoulos, V., Selli, E., Lianos, P., 2016. Highly functional titania nanoparticles produced by flame spray pyrolysis. Photoelectrochemical and solar cell applications. *Appl. Catal. B*, 182, 369–374. <https://doi.org/10.1016/j.apcatb.2015.09.040>.
- Tsubota, S., Haruta, M., Kobayashi, T., Ueda, A., Nakahara, Y., 1991. Preparation of Highly Dispersed Gold on Titanium and Magnesium Oxide. *Stud. Surf. Sci. Catal.* 63, 695–704. [https://doi.org/10.1016/S0167-2991\(08\)64634-0](https://doi.org/10.1016/S0167-2991(08)64634-0).
- Velempini, T., Prabakaran, E., Pillay, K., 2021. Recent developments in the use of metal oxides for photocatalytic degradation of pharmaceutical pollutants in water—a review. *Mater. Today Chem.* 19, 100380 <https://doi.org/10.1016/j.mtchem.2020.100380>.
- Watanabe, M., 2017. Dye-sensitized photocatalyst for effective water splitting catalyst. *Sci. Technol. Adv. Mater.* 18, 705–723. <https://doi.org/10.1080/14686996.2017.1375376>.
- Wenderich, K., Mul, G., 2016. Methods, Mechanism, and Applications of Photodeposition in Photocatalysis: A Review. *Chem. Rev.* 116, 14587–14619. <https://doi.org/10.1021/acs.chemrev.6b00327>.
- Wu, J., Ma, X., Xu, L., Zhao, B., Chen, F., 2019. Fluorination promoted photoinduced modulation of Pt clusters on oxygen vacancy enriched TiO<sub>2</sub>/Pt photocatalyst for superior photocatalytic performance. *Appl. Surf. Sci.* 489, 510–518. <https://doi.org/10.1016/j.apsusc.2019.05.304>.
- Xie, S., Wang, Yu., Zhang, Q., Deng, W., Wang, Y.e., 2014. MgO- and Pt-promoted TiO<sub>2</sub> as an efficient photocatalyst for the preferential reduction of carbon dioxide in the presence of water. *ACS Catal.* 4, 3644–3653. <https://doi.org/10.1021/cs500648p>.
- Yan, M., Li, G., Guo, C., Guo, W., Ding, D., Zhang, S., Liu, S., 2016. WO<sub>3-x</sub> sensitized TiO<sub>2</sub> spheres with full-spectrum-driven photocatalytic activities from UV to near infrared. *Nanoscale*, 8 (2016), 17828–17835. <https://doi.org/10.1039/c6nr06767k>.
- Zanella, R., Giorgio, S., Henry, C.R., Louis, C., 2002. Alternative methods for the preparation of gold nanoparticles supported on TiO<sub>2</sub>. *J. Phys. Chem. B* 106, 7634–7642. <https://doi.org/10.1021/jp0144810>.
- Zhang, H., Chen, B., Banfield, J.F., Waychunas, G.A., 2008. Atomic structure of nanometer-sized amorphous TiO<sub>2</sub>. *Phys. Rev. B Condens. Matter. Phys.* 78, 214106 <https://doi.org/10.1103/PhysRevB.78.214106>.
- Zhang, P., Ran, Y., Tan, J., Xie, H., Wang, J., Ding, S., 2020. Photodeposition of Pt on the Bi<sub>2</sub>WO<sub>6</sub> nanosheets under irradiation of 365 nm and 450 nm LED lights. *Chem. Phys. Lett.* 739, 137019 <https://doi.org/10.1016/j.cplett.2019.137019>.
- Zielińska-Jurek, A., Wei, Z., Wysocka, I., Szweda, P., Kowalska, E., 2015. The effect of nanoparticles size on photocatalytic and antimicrobial properties of Ag-Pt/TiO<sub>2</sub> photocatalysts. *Appl. Surf. Sci.* 353, 317–325. <https://doi.org/10.1016/j.apsusc.2015.06.065>.